ELSEVIER

Journal of Non-Crystalline Solids 289 (2001) 175–184

JOURNAL OF NON-CRYSTALLINE SOLIDS

www.elsevier.com/locate/jnoncrysol

The effects of radiation on the density of an aluminoborosilicate glass

M.O. Prado [a,*,1], N.B. Messi [b], T.S. Plivelic [c], I.L. Torriani [c,d], A.M. Bevilacqua [b], M.A. Arribére [b]

[a] *Departmento de Engenharia de Mat. (LAMAV), Universidade Federal de São Carlos, Via Washington Luiz km 235, Caixa Postal 676, 13565-905 São Carlos-SP, CEP, Brazil*

[b] *Centro Atómico Bariloche, CNEA, S.C. de Bariloche, Argentina*

[c] *Laboratorio Nacional de Luz Síncrotron, Campinas, SP, Brazil*

[d] *Instituto de Física 'Gleb Wataghin', UNICAMP, Campinas, SP, Brazil*

Received 16 January 2001

Abstract

Glasses used for nuclear waste immobilization are subjected to high levels of radiation, and this may affect their physicochemical properties. Alpha radiation is responsible for an important fraction of the radiation energy dissipated in these glasses. It has been reported previously that some borosilicate glasses increase their density during irradiation while the density of other glasses decreases. Although the density increase of silica after irradiation has been understood, thanks mainly to molecular dynamics calculations and diffraction experiments, the processes involved in more complex glasses could be more varied. In this work we irradiated an aluminum-borosilicate glass which is a candidate for the aforementioned purposes and which increases density during alpha irradiation from the ^{10}B (n,α) ^{7}Li reaction. We studied the effects of alpha irradiation on its microstructure, using several experimental techniques, and subsequently correlated the results. Small angle X-ray scattering (SAXS) measurements revealed the presence of inhomogeneities of about 10 Å in the untreated samples. After annealing these samples, TEM images displayed a contrast structure and helium pycnometry revealed density changes, both typical of glass phase separation. After irradiation, the glass density increased and the SAXS intensity decreased, indicating a compositional homogenization process in the samples subject to a higher dose of irradiation. Atomic displacements were calculated by means of the TRIM [1] computer code. The number of displacements produced by each ^{10}B(n,α) ^{7}Li reaction was estimated at 580 and involved distances of up to 15 Å. An increase in the density of the irradiated samples can be explained in terms of the atomic displacements produced by the nuclear reaction cascades of the reaction ^{10}B (n,α) ^{7}Li, in the scenario of pre-existing phase separation in the samples. In the case of the aluminum-borosilicate glasses studied here, which exhibit a fine phase separation, the density of the Si-rich phase increases with the incorporation of Na and B atoms. The B-rich phase also increases its density with the flow of Si atoms from the matrix. Vacancies created by irradiation in the glass structure, are responsible for a density decrease. The final effect is due to the sum of all contributions described, which in this case results in a net density increase of the irradiated samples. An understanding of this phenomenon can lead to the design of new glasses which overcome radiation with a minimum of density change.

* Corresponding author. Fax: +55-2944 445 299.

E-mail address: pradom@cab.cnea.gov.ar (M.O. Prado).

[1] On leave from the Comisión Nacional de Energía Atómica, Centro Atómico Bariloche, 8400-S.C. de Bariloche, Argentiana.

0022-3093/01/$ - see front matter
PII: S0022-3093(01)00707-4

1. Introduction

The effect of densification of glasses by high energy particles such as fast neutrons, alpha particles or recoil nucleus has been extensively studied and is well known. Vitreous silica irradiated with a fast neutron dosage of 2×10^{19} neutrons/cm^2 densifies 2–3%. Further irradiation to 2×10^{20} neutrons/cm^2 causes dilation, with a partial recovery of the densification effect [2]. Bates et al. [3] also found a 2% densification of vitreous silica when irradiated with 5×10^{19} neutrons/cm^2, and a 16% decrease in the density of α-quartz when irradiated with 9×10^{19} neutrons/cm^2. Mendel et al. [4] found a density increase of 0.5% in a zinc-borosilicate glass doped with ^{244}Cm, which is an alpha emitter.

Marples [5] studied the dose rate effects of radiation damage to vitrified radioactive waste. Five borosilicate compositions were doped with ^{238}Pu. One of them increased its density and the other glasses showed a density decrease when irradiated with ^{238}Pu α-decay.

Sato et al. [6] studied density changes in four borosilicate glasses. When subjected to the ^{10}B (n,α) ^{7}Li nuclear reaction, one of them suffered an increase in density and the others exhibited a density decrease. Messi et al. [7] found an increase of about 1% in the aluminum-borosilicate glass density after irradiation with thermal neutrons and the products of the reaction ^{10}B (n,α) ^{7}Li (Fig. 1).

The authors also reported complete, or almost complete, reversibility of the density changes caused by radiation by subsequent thermal treatments. Marples [5] made a thorough study of the density recovery in five borosilicate glasses. He reported that depending upon the glass composition, the recovery could be partial or total, annealing the irradiated glasses for long periods.

In all cases, several authors [3–7] agree that the most important processes that play a role in volume change, mainly those which generate a density increase during irradiation, are not clear. The aim of this work is to determine which are the processes, that cause the density changes in the different glass systems during irradiation.

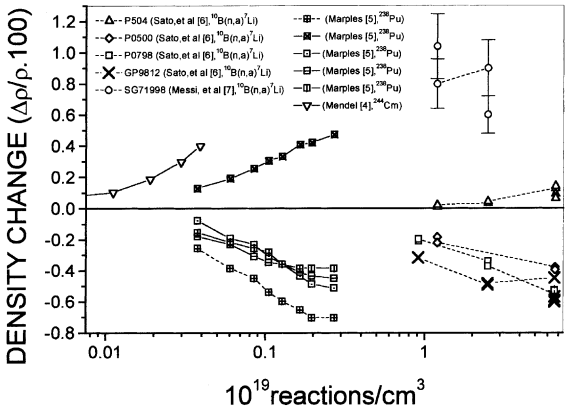

Fig. 1. Density change vs. reactions/cm^3 for different glasses as measured by Mendel et al. [4], Marples [5], Sato et al. [6] and Messi et al. [7]. In each case different nuclear reactions and therefore different dissipated energy per reaction were used. Lines are only a guide to the eye.

2. Experimental procedures and calculations

2.1. Phase separation in the splat-cooled glass samples

The glass chosen for this work was the aluminoborosilicate glass (hereafter SG7 glass) since it presented a marked increase in its density during irradiation [7]. Its composition is wt% : SiO_2 71.7, B_2O_3 8.33, Al_2O_3 8.56, MgO 1.00, CaO 2.67, Na_2O 7.44.

Glass samples were prepared by heating the glass up to 1923 K. Then the melted glass was poured and pressed between two stainless steel plates (splat-cooled), in order to minimize phase separation during sample preparation. Transparent, non-colored samples a few millimeters thick were obtained by this technique. To confirm the presence of phase separation in this glass, which later will be the key to explain the density increase after irradiation, isothermal treatments were made at 998 K, and the evolution of phase separation was studied by observation of opalescence, density measurements, and transmission electron microscopy. X-ray diffraction (XRD) was used to determine the appearance of crystalline phases.

2.2. Sintered glass samples: preparation, irradiation, SAXS measurements

Cylindrical samples of the powder glass SG7, were obtained following the same procedures used for the preparation of glasses intended to immobilize nuclear wastes. First, uniaxially pressing the powder in a die at 1 kg/cm^2, their green density being approximately 1.45 g/cm^3. They were sintered at 998 K during 3 h. Heating and cooling rates of 5 K/min were used. They had a final density measured by immersion in water of 2.32 g/cm^3 which was 97% of the theoretical density. From the cylindrical samples, ten slabs were cut, ground until 150 μm thick, and polished on both sides with 6 μm diamond paste. Two samples were kept without irradiation as reference.

Eight other samples were irradiated by pairs with the four different neutron fluences listed in Table 1, at the nucleus of the reactor RA6 (Research Argentine Reactor No. 6, S.C. de Bariloche, Argentina). Samples were placed in an aluminum capsule. Aluminum foils were placed between samples and between samples and capsule to ease heat dissipation from the samples towards the capsule walls. Tin chips 6 N pure, were set among the samples as indicators that the temperature during irradiation did not reach the Sn melting point, namely 505 K.

Although the ^{10}B neutron capture cross-section is high for thermal neutrons, the thermal neutron flux is inevitably accompanied by epithermal and fast neutron fluxes. The thermal, epithermal and fast neutron fluxes, to which the samples were subjected, were measured using activation detectors.

Thermal and epithermal fluxes were measured as described in [8], using an Al–Co alloy (Co content 0.491 wt%) [9] and a deposition of $AgNO_3$ solution on filter paper, respectively.

The fast neutron flux was measured with Ni as monitor, considering an energy spectrum of neutrons corresponding to that of the thermal fission of ^{235}U. The used nuclear parameters were taken from standard tables [10–14].

2.3. SAXS measurements and data analysis

Phase separation in the sintered glass samples, before and after the irradiation of the glass with thermal neutrons and the products of the reaction ^{10}B(n,α) ^{7}Li was characterized by small angle X-ray scattering (SAXS).

For a system of polydispersed particles (inhomogeneities or scattering centers) within a matrix, with a contrast in its electronic density $\Delta\rho$, diluted and isotropic, the scattered X-ray intensity $I(q)$ can be expressed as

$$I(q) = \int_{R_{\min}}^{R_{\max}} g(R) I_1(q,R)\,\mathrm{d}R, \tag{1a}$$

where $g(R)$ is the distribution of particles' sizes and $\int_{R_{\min}}^{R_{\max}} g(R)\,\mathrm{d}R = n$, with n the density of particles per unit volume and $I_1(q,R)$ is the scattered intensity originated by one particle. $I_1(q,R)$ can be expressed as

$$I_1(q,R) = \Delta\rho^2 v(R)^2 f(q,R)^2, \tag{1b}$$

where v is the particle's volume and $f(q,R)$ is a geometrical shape factor [15].

In our experiments, the synchrotron light source of the Brazilian National Synchrotron Light Laboratory (LNLS) was used, with $\lambda = 1.608$ Å, at a sample–detector distance =

Table 1
Neutron fluences and calculated reactions corresponding to different irradiated samples

Sample pair	Thermal neutron fluence (10^{17} cm^{-2})	Epithermal neutron fluence (10^{15} cm^{-2})	Fast neutron fluences (10^{16} cm^{-2})	Calculated ^{10}B (n,α) ^{7}Li reactions (10^{17} cm^{-3})
1	1.71 ± 0.05	7.0 ± 0.7	5.3 ± 0.2	4.30
2	3.48 ± 0.11	13.4 ± 1.3	10.7 ± 0.4	8.81
3	4.52 ± 0.12	14.9 ± 1.8	13.4 ± 0.4	11.44
4	11.35 ± 0.34	44.0 ± 4.2	31.6 ± 1.0	28.73

571.03 mm which allowed the measurements of the scattered radiation from $q = 0.01\ \mathrm{A}^{-1}(q_{\min})$ up to $q = 0.5\ \mathrm{A}^{-1}(q_{\max})$. The general experimental setup is described in [16].

For each scattering curve measured, the intensity was corrected for standard instrumental factors as well as for sample attenuation. The background intensity was subtracted fitting a second-order polynomial for the Porod region (i.e. for high values of the scattering vector q) according to Eq. (2) [17]:

$$I(q)_{q\to\infty} \approx \frac{K_{\mathrm{P}}}{q^4} + \beta_0 + \beta_1 q^2, \tag{2}$$

where K_{P} is the Porod constant, β_0 and β_1 are the constants related to the background intensity. All three constants were determined by fitting Eq. (2) to the experimental curves. The Porod invariant Q, was calculated using Eq. (3) and following the procedures detailed in [18]:

$$Q = \int_0^\infty I(q) q^2 \,\mathrm{d}q. \tag{3}$$

For a polydisperse system of spherical particles the invariant Q and the Porod constant K_{P} are related to a moment of the mean particle radius R according to Eq. (4). The quantity $\langle R^3\rangle/\langle R^2\rangle$, often called the Porod radius R_{P}, represents an average dimension of the scattering centers.

$$R_{\mathrm{P}} = \frac{\langle R^3\rangle}{\langle R^2\rangle} = \frac{3Q}{\pi K_{\mathrm{P}}}. \tag{4}$$

In order to obtain the particle size distribution, a standard program (GNOM [19]) was used to calculate the volumetric size distribution functions for the different irradiated samples, assuming the existence of one population of spherical particles. To check the validity of the distribution obtained with the GNOM program special attention was given to: (1) the quality of the fit of the calculated intensity to the measured intensity, (2) the agreement of the Porod radius R_{P} (calculated using Eq. (4)) with the R value corresponding to the maximum of the size distribution curve, and (3) the agreement of the Porod radius R_{P} with the value $\langle R^3\rangle/\langle R^2\rangle$ calculated from the volume distribution of particles with radius R, $V(R)$ obtained from GNOM as indicated in Eq. (5):

$$\frac{\langle R^3\rangle}{\langle R^2\rangle} = \frac{\int_0^\infty V(R) R^3 \,\mathrm{d}R}{\int_0^\infty V(R) R^2 \,\mathrm{d}R}. \tag{5}$$

2.4. TRIM calculations

The radiation damage caused to the glass by the α-decays and Li-recoils from the ^{10}B(n,α) ^{7}Li nuclear reaction, consists mainly in heavily damaged zones around their tracks (cascades), and the build up of damage involves the increase in the number of such zones in the glass.

The TRIM computer code was used to calculate the cascade corresponding to each nuclear reaction ^{10}B (n,α) ^{7}Li. Energies of 1.8 MeV for the alpha particles and 1 MeV for the Li ions, binding energies of 2 eV and an energy threshold for atomic displacement of 20 eV, were used during the calculations. The glass composition was simplified to $14Na_2O \cdot 14B_2O_3 \cdot 72SiO_2$.

The cascade is characterized mainly by the following calculated quantities: Ion longitudinal and transversal range, ion energy dissipated in creating vacancies, recoil energy dissipated in creating vacancies, space distribution of each type of displaced atoms excluding atom replacements, space number distribution of vacancies and space distribution of the energy dissipated in each type of atoms.

3. Results

3.1. Phase separation of the splat-cooled SG7 glass

The sample annealed at 998 K exhibited a slight bluish opalescence typical of phase separation. The opalescence increased as a function of annealing time. After 45 h the opalescence was evident with the naked eye and after about 300 h the samples became milky.

Fig. 2 shows the microstructure observed with TEM for the glass after 310 h of thermal treatment at 998 K. A connected two-phase structure is found, with typical size of a few nanometers. XRD

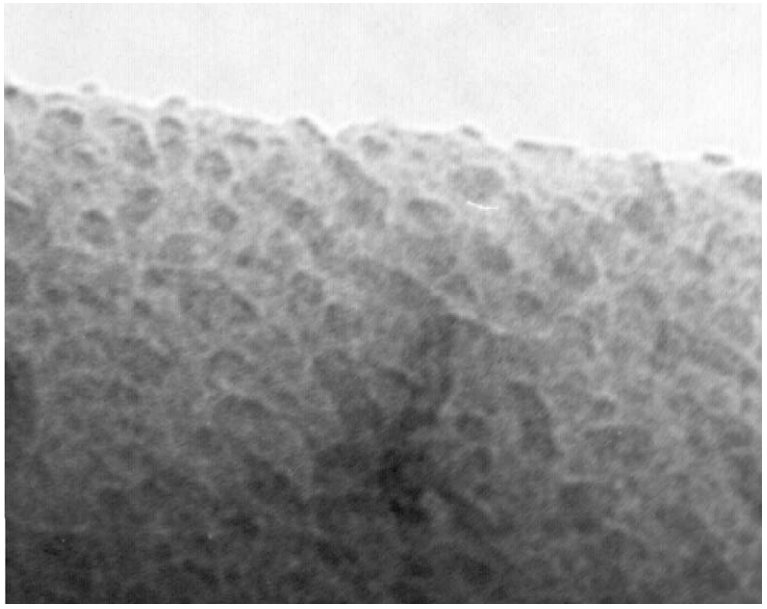

Fig. 2. TEM photograph corresponding to the glass after 310 h thermal treatment at 998 K (TEM analysis carried out at the Laboratorio de Caracterização Estrutural – DEMA-UFSCAR with a Philips CM 120 TEM). The image was obtained on a thin region of crushed particles. Photograph width: 150 nm.

spectra corresponding to the sample of Fig. 2, exhibits a glassy structure, indicating that no crystallization occurred during the thermal treatment.

Fig. 3 shows the evolution of the glass density during phase separation at 998 K, as measured with a helium pycnometer. The density decreases about 0.5% in the first hour, and after that it becomes stable, this density plateau is accompanied by a strong increase in opalescence which is assigned to the coalescence of smaller particles of the dispersed phase.

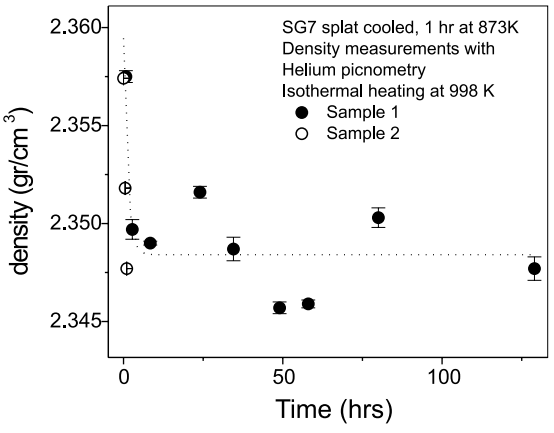

Fig. 3. Evolution of the glass density during phase separation at 998 K, as measured with a helium pyknometer. Dashed line is only a guide to the eye.

Both new glassy phases are expected to be less compact than the original 'homogeneous' glass since the following facts are known: silica glasses increase their density when alkaline ions or B are incorporated into their network and vice-versa [20].

3.2. Phase separation in the sintered SG7 glass samples

During the thermal treatment for sintering, a fine phase separation structure is developed in the samples, which can be studied by SAXS.

Fig. 4 shows a typical SAXS curve for the sintered glass SG7, plotted as $\ln(I)$ vs. q^2. It is found that the region of small q values did not have a linear behavior, indicating polydispersity and a particle size distribution. These features are common to non-irradiated and to irradiated samples. Fig. 5 shows a typical fit of the measured scattered

Table 2
Comparison of the Porod radius R_P, the radius corresponding to the maximum volume of particles obtained with GNOM R_{max}, and the Porod radius $\langle R^3\rangle/\langle R^2\rangle$ calculated with the particle size distribution obtained with GNOM

Sample	R_P(Porod) (Å) ±0.3 Å	R_{max}(GNOM) (Å) ±1.1 Å	Calculated$\langle R^3\rangle/\langle R^2\rangle$ (Å) ±1.3 Å
B3	9.7	9.8	9.7
B4	10.4	8.4	9.9
B5	9.7	8.0	8.0
B6	9.8	10.4	10.4
B7	9.8	8.0	7.4

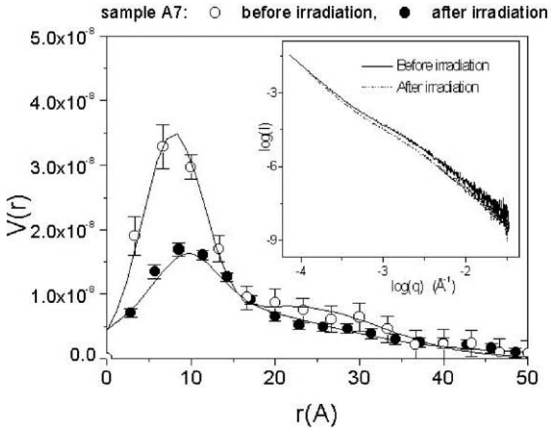

Fig. 7. Calculated distributions of particle sizes before and after irradiation with maximum fluence. Inset: SAXS intensities from which the size distributions were obtained.

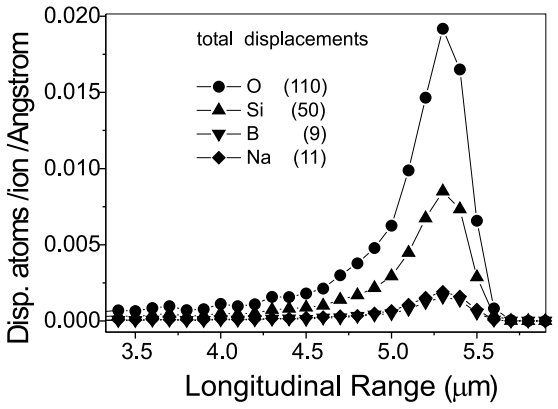

Fig. 8. Displaced atoms/ion/Å vs. distance from glass surface, ion beam perpendicular to glass surface. Distance measured in the direction of the beam.

recoil atoms. Li atoms dissipate 0.02% of their energy in generating vacancies and 2.33% is transferred to recoil atoms. Although the ion (alpha and Li ions) ranges are of the order of micrometers the recoil atoms (Si, O, B, Na) generated in each cascade have ranges, estimated with TRIM, less than 15 Å. This range for recoil atoms, although small, is sufficient to displace many of the atoms from the particles whose dimensions are approximately 10 Å.

4. Discussion

Displacement of atoms from their positions in the glass network, caused by irradiation cascades, can give rise to a number of structural changes. When vitreous silica is irradiated a density increase occurs due to a change in the distribution of Si–O ring sizes as demonstrated by [22].

We propose that, in glasses with phase separation or physical inhomogeneities, apart from the change in the distribution of Si–O ring sizes, other processes can contribute to the density change in these glasses. We know from the literature that one of the glassy phases present in borosilicate with phase separation is enriched in B and Na and the second glassy phase is enriched in Si [23,24].

Table 4 lists, for the alumino-borosilicate studied here, the different atomic processes associated to the displaced ion's (glass former or glass modifier) and their possible effect on the bulk density (↓: density decrease, ↑: density increase).

We propose that density changes during irradiation are associated with the generation of vacancies and also with an effective transport of atoms between inhomogeneities or separated phases of the glass and the matrix. This transport will be more effective when the size of inhomogeneities is of the order of the range of displaced

Table 3
Characterization of a ^{10}B (n,α) ^{7}Li cascade

	Range (μm)	Straggle (μm)		Range (μm)	Straggle (μm)	
	Alpha particles: vac/ion = 180			*Li ions: vac/ion = 363*		
Longitudinal	5.29	0.16		2.47	0.18	
Lateral	0.20	0.26		0.19	0.25	
% energy	Ions	Recoils		Ions	Recoils	
	Alpha particles: 1.8 MeV			*Li ions: 1 MeV*		
Ionization	99.45	0.15		97.5	0.98	
Vacancies	0.01	0.01		0.02	0.05	
Phonons	0.06	0.41		0.14	1.30	
Displaced atom	$\langle E\rangle$/ion (eV)	Range (Å) Less than	Number of displaced atoms/ion	$\langle E\rangle$/ion (eV)	Range (Å) Less than	Number of displaced atoms/ion
	Alpha particles: 1.8 MeV			*Li ions: 1 MeV*		
O	57	15	110	66	15	221
Si	65	15	50	71	15	101
B	39	15	9	42	15	18
Na	50	15	11	54	15	23

Calculations made with TRIM. Alpha particles (1.8 MeV) and Li ions (1 MeV) in a borosilicate glass.

atoms. For the glass composition studied in this work, phase separation gives rise to inhomogeneities, with a size distribution peaked at about 10 Å, as our results from SAXS show in Fig. 6.

From TRIM calculations we learned that the range of displaced B, Na and Si atoms is about 10–15 Å, allowing B and Na atoms to migrate from the B- and Na-rich regions to the Si-rich matrix. The latter is experimentally proved by the fact that at high radiation doses, the small angle scattered X-ray intensity decreases, indicating a decrease in the electron density contrast between the matrix and the dispersed phase (See Fig. 7 and Eq. (1a) and (1b)) or a decrease in the number of the X-ray scattering centers. It is known that, for all binary alkaline silicates, the incorporation of the alkaline ions into the reticular holes originates a higher mass concentration (compared to that of vitreous silica) with sometimes a small increase in volume, and a concomitant density increase [23,24]. (Process 8 in Table 4.)

The molar replacement of SiO_2 by B_2O_3 produces a decrease of the partial volume of oxygen, since the boric anhydride possesses a more compact structure than that of vitreous silica, due to the higher field intensity (Process 4 in Table 4) of the B^{3+} ion. Moreover, the transport of Si atoms from the matrix towards the B, Na reach particles, decreases electrostatic repulsion among $BO^{-}_{4/2}$ glass atomic aggregates [24]. (Process 5 in Table 4.) Then events of the type 4, 5 and 8 dominate over processes 1,2,3, 6 and 7 resulting in a glass density increase. We note in Fig. 3, that density decreases with phase separation. Radiation cascades, with an effective ion transport among phases homogenizes the glass, and the density increases.

Thermal treatment should reverse the effect of radiation, allowing phase separation, leading to a new decrease in density. This would be the cause for the thermal reversibility effect in glasses with phase separation. Nevertheless the structure of the separated phases, depends on whether the temperature of annealing is lower or higher than the immiscibility temperature of the metastable liquid-phases and on annealing time [24]. In an ideal 'homogeneous' glass, density changes due to radiation could only involve processes 1, 2, 3, 6 and 7 listed in Table 4.

If that homogeneous glass, did not include any modifier, only 1,2 and 3 remain as possible events. This is the case for vitreous silica, which has a very open structure, as we conclude by comparing the density of vitreous silica 2.20 g/cm^3 with that of α-quartz 2.64 g/cm^3 [5]. Vitreous silica accommo-

Table 4
Some possible processes that can produce glass density change during irradiation of the alumino-borosilicate studied in this work

Atom type	Mechanism considered	Observation	ρ
Glass former	1 – Atom is displaced from its position in the glass network by ion or other recoils, a 'vacancy' is created	• Always occurs	↓
Glass former	2 – Displaced atom, ends its trajectory in an interstitial (crystal's interstitial-like) position	• Occurs associated to mechanism 1	↓
Glass former	3 – Displaced atom ends its trajectory in an opened site of the same glass former	• Occurs associated to mechanism 1 • Needs an open structure • Needs inhomogeineties to result in a preferential direction • Range of recoils > inhomogeneities size[a]	↑
Glass former	4 – Displaced atom ends its trajectory in an opened site of a different glass former (B incorporates in SiO_2 glass)	• Occurs associated to mechanism 1 • Needs phase separation • Range of recoils > inhomogeneities size (some borosilicate glasses)	↑
Glass former	5 – Displaced atom ends its trajectory and incorporates to other oxide glass decreasing electrostatic repulsion among atomic aggregates (Si incorporates in $BO^{-}_{4/2}$ glass)	• Needs phase separation • Range of recoils > inhomogeneities size	↑
Glass modifier	6 – Atom is displaced from its position in the glass network by ion or other recoils, a vacancy is created	• Always occurs	↓
Glass modifier	7 – Displaced atom, ends its trajectory in an interstitial (crystal's interstitial-like) position	• Occurs associated to mechanism 6	↓
Glass modifier	8 – Displaced atom ends its trajectory in an open site within a different glass composition (Na from the B/Na-rich particles incomes the Si-rich matrix)	• Occurs associated to mechanism 6 • Needs phase separation to result in a preferential direction • Range of recoils > inhomogeneities size	↑

(↓: density decrease, ↑: density increase).
[a] Note that range of recoils (Si, O, B, Na) is not range of ions (alpha,Li).

dates 17% less mass than α-quartz. During irradiation with fast neutrons, silica density increases 2–3% [5]. Then, the prevailing effect is that due to mechanism 3 in Table 4. Although silica is one of the best studied materials, there are some aspects of its structure which still remain to be elucidated, as the presence of large scale inhomogeneities with sizes of about 10 000 Å according to SAXS measurements [25]. In short, a density increase could only happen in the presence of chemical inhomogeneities (phase separation) or physical inhomogeneities (open structure of vitreous silica).

5. Conclusions

From the results obtained in this work, we can propose a number of processes that play a role in the density change during the irradiation of an alumino-borosilicate glass which exhibits glass phase separation. Some of them promote a density decrease, others a density increase. During irradiation they exist simultaneously and the balance of all these effects will decide if density increases or decreases.

The atomic processes identified as responsible for the final structure are: creation of 'vacancies', 'interstitials' and the associated matter transport through inhomogeneities or different phases of the sample. If recoil ranges are of the order or greater than the typical size of the inhomogeneities, these inhomogeneities will tend to disappear as a consequence of cascades. For each type of particle, the irradiation effect on the density of the glasses must be studied.

For borosilicate glasses without phase separation we expect a density decrease after irradiation.

For borosilicate glasses with phase separation, we have to consider two cases: (1) if there is a fine phase separation, there is a density increase. (2) if the typical size of the inhomogeneities is considerably greater than the ranges of the recoil atoms, we expect a decrease in density. The thermal damage recovery expected depends on whether the same metastable liquid phase separation is accomplished or not.

Further research would be welcome in this field, leading to the design of glasses with the desired response to irradiation by controlling phase separation or the size distribution of inhomogeneities.

Acknowledgements

Helpful discussions with Professsor Dr Edgar Zanotto and sample preparation by Mr Miguel Sanfilipo are greatly acknowledged. We are thankful to Dr Paulo Cesar Soares Jr for obtaining the TEM images. This work has been partially funded by the Consejo Nacional de Investigaciones Científicas y Técnicas (Argentina), the Comisión Nacional de Energía Atómica (Argentina) and the Laboratorio Nacional de Luz Síncrotron (Campinas-Brasil) through project #488-99.

References

[1] J.F. Ziegler, J.P. Biersack, O. Littmark, in: J.F. Ziegler (Ed.), The Stopping and Range of Ions in Solids, vol. 1, Pergamon, New York, 1985 (Chapter 4).
[2] W. Primak, J. Phys. Chem. Glasses 10 (3) (1960) 117.
[3] J.B. Bates, R.W. Hendricks, L.B. Shaffer, J. Chem. Phys. 61 (10) (1974) 4163.
[4] J.E. Mendel, W.A. Ross, F.P. Roberts, R.P. Turcotte, Y.B. Katayama, J.H. Westsik, in: Proceedings of the IAEA Symposium IAEA-SM-207/100, 1976, p. 49.
[5] J.A.C. Marples, Nucl. Instrum. and Meth. B 32 (1988) 480.
[6] S. Sato, H. Furuya, T. Kozaka, Y. Inagaki, T. Tamai, J. Nucl. Mater. 152 (1988) 265.
[7] N. Messi de Bernasconi, M. Prado, A. Bevilacqua, M. Arribere, Daño por radiación alfa en bloques vítreos sinterizados, Congresso Geral de Energía Nuclear, Brasil, 1998.
[8] M.A. Arribére, A.J. Kestelman, in: Selected topics about applications of the k-sub-zero and other parametric methods in Neutron Activation Analysis, Report of the International Atomic Energy Agency, p. 89.
[9] Supplier: Reactor Experiments Inc.
[10] Nuclear Analysis Software, Part 2, IAEA, Vienna, IAEA/CMS/3, 1991.
[11] K.J. Tuli, Nuclear Wallet Cards, National Nuclear Data Center, Brookhaven National Laboratory, 1995.
[12] R.B. Firestone, V. Shirley, Table of Isotopes, Wiley, New York, 1996.
[13] M. Mughabghab, M. Divadeenam, N.E. Holden, Neutron Cross Sections, Neutron Resonance Parameters and Thermal Cross Sections, vol. I, Part A Z = 1–60, Academic Press, New York, 1981.
[14] M. Mughabghab, Neutron Cross Sections, Neutron Resonance Parameters and Thermal Cross Sections, vol. II, Part A Z = 61–100, Academic Press, New York, 1984.
[15] O. Glatter, O. Kratky, Small Angle X-ray Scattering, Academic Press, New York, 1982.
[16] G. Kellerman, F. Vicentin, E. Tamura, M. Rocha, H. Tolentino, A. Barbosa, A. Craievich, I. Torriani, J. Appl. Cryst. 30 (1997) 880.
[17] C.G. Vonk, J. Appl. Crystallogr. 6 (1973) 81.
[18] I.S. Patel, P.W. Schmidt, J. Appl. Crystallogr. 4 (1971) 50.
[19] D.I. Svergun, J. Appl. Crystallogr. 25 (1992) 495.
[20] José Maria Fernandez Navarro, El Vidrio, Taravilla, Madrid, 1991, p. 373 (Chapter 10).
[21] A. Varsshneya, Fundamentals of Inorganic Glasses, Academic Press, New York, 1994 (Chapter 4).
[22] J. Wein, K.K. Rajiv, P. Vashishta, J.P. Rino, Phys. Rev. B 50 (1) (1994) 118.
[23] A. Varsshneya, Fundamentals of Inorganic Glasses, Academic Press, New York, 1994 (Chapter 5).
[24] Jesús Rincón, Alicia Durán, Separación de Fases en Vidrios, Monograph of the Sociedad Española de Cerámica y Vidrio, Artes Gráficas Ibarra, Madrid, 1982 (Chapter 5).
[25] E.A. Porai Koshits, Ann. Rev. Mater. Sci. 6 (1976) 389.